# FISEVIER

Contents lists available at ScienceDirect

# Carbon

journal homepage: www.elsevier.com/locate/carbon



# Controllable inversion symmetry breaking in single layer graphene induced by sub-lattice contrasted charge polarization



Beibei Shi <sup>a</sup>, Yingdong Xiao <sup>a</sup>, Tianyang Han <sup>a</sup>, Haotian Cheng <sup>a</sup>, Jincan Zhang <sup>b, c</sup>, Qiao Jiang <sup>a</sup>, Hailin Peng <sup>b</sup>, Han Zhang <sup>a</sup>, Xing Zhu <sup>a</sup>, Zheyu Fang <sup>a, \*</sup>

- <sup>a</sup> School of Physics, State Key Lab for Mesoscopic Physics, Academy for Advanced Interdisciplinary Studies, Collaborative Innovation Center of Quantum Matter, Nano-optoelectronics Frontier Center of Ministry of Education, Peking University, Beijing, 100871, PR China
- <sup>b</sup> Center for Nanochemistry, Beijing Science and Engineering Center for Nanocarbons, Beijing National Laboratory for Molecular Sciences, College of Chemistry and Molecular Engineering, Peking University, Beijing, 100871, PR China
- <sup>c</sup> Academy for Advanced Interdisciplinary Studies, Peking University, Beijing, 100871, PR China

#### ARTICLE INFO

#### Article history: Received 4 December 2019 Received in revised form 20 February 2020 Accepted 7 March 2020 Available online 9 March 2020

#### ABSTRACT

It has been revealed that inversion symmetry breaking in graphene could induce non-trivial Berry curvature, which leads to topologically protected valleytronic applications. Here, we propose an active controllable way of realizing the inversion symmetry breaking of single layer graphene, which is induced by the contrasted AB sub-lattice charge polarization. Our theory model indicates the split of in-plane optical phonons (iTO/iLO) at  $\Gamma$  point is the direct result of inversion symmetry breaking in single layer graphene. Density functional theory calculation was used to quantify the sub-lattice charge polarization and the split of iTO/iLO phonons under the external in-plane electric field, which was further confirmed by Raman spectroscopy. We believe that the method of symmetry manipulation by external in-plane electric field advances fundamental comprehension for the inner mechanism of topological phase transition of graphene.

© 2020 Elsevier Ltd. All rights reserved.

## 1. Introduction

Current studies in two-dimensional (2D) materials have revealed that the non-trivial topological phase could lead to optical and electrical properties like tunable bandgap [1], valley contrasted circular dichroism [2], etc., which could be utilized for the application of spintronic and valleytronic devices [3,4]. Berry curvature [5] can be used to quantify the topological property of parameter space. In the topological trivial parameter space, Berry curvature should be zero everywhere, while in a topological non-trivial space, it would have a non-zero value somewhere therefore some of the adiabatic evolution paths of electrons could have non-trivial geometric phases. Because the effect of the non-trivial geometric phase is difficult to be measured directly, researchers proposed several methods to reflect the effect of non-trivial topological property of materials, like using angle resolved photoemission spectroscopy (ARPES) to characterize the edge state of a topological insulator [6], and to measure the anomalous quantum Hall effect [7], etc..

\* Corresponding author. E-mail address: zhyfang@pku.edu.cn (Z. Fang).

Because of the high carrier mobility and convenient manipulation of Fermi level and carrier density [8,9], graphene becomes a potential alternate of novel semi-conductive material [10]. Although intrinsic graphene, due to its chiral symmetry between A and B sub-lattices, is a topological trivial material, researchers have developed kinds of methods to decrease the chiral symmetry by breaking its time-reversal symmetry or inversion symmetry. The former time-reversal symmetry breaking could lead to edge bands cross the energy gap and make graphene as a topological insulator, which often realized by applying a perpendicular magnetic field into the single layer graphene (SLG) [11]. However, the weak spinorbit coupling in the graphene makes it difficult to induce and detect the symmetry broken. To apply a perpendicular external electric field is a common method to realize the breaking of inversion symmetry for the double layer graphene [12]. For the SLG, it needs to induce a staggered on-site energy on the sub-lattices, which is often realized by adding substrates like hexagonal Boron-Nitride [13] and SiC(0001) [14], however the manipulation of substrates is lack of controllability.

In this letter, we propose an active controllable way to induce the non-trivial Berry curvature and overcome the shortcoming of above chiral symmetry breaking methods by applying an external in-plane electric field to break the inversion symmetry of SLG. This method may break the single-layer graphene zero band gap, making it semiconductor material, and even with the phenomenon of valley polarization. That is, we may realize artificial valley polarized materials by this method. The in-plane electric field induced relative polarization of sub-lattice A and B changes the symmetry at  $\Gamma$  point from  $D_{6h}$  to  $D_{2h}$ , leading to the non-trivial Berry curvature and a split of the degenerated energy level of iLO and iTO phonons at  $\Gamma$  point. We study the relationship between the relative polarization and the split of the G peak analytically, and the established relationship can be further directly measured by using Raman spectroscopy, where the split of G peak actually represents the change of the topological property of graphene, which is induced by symmetry broken. We calculated the polarization charge under the field using the method of density functional theory (DFT) and carried out a specially designed experiment to verify the existence of the in-plane electric field induced polarization. We reveal that in-plane external electric field can be used to break the chiral symmetry of intrinsic graphene and might make it topological non-trivial material.

#### 2. Theoretical section

2.1. Theoretical model: optical phonons split of SLG under electric field

In the case of single layer graphene, the equations of motion in the harmonic approximation are written in the form of [15,16].

$$\sum_{i,m,\kappa'} \varphi_{ij}^{\kappa\kappa'}(\boldsymbol{a_n} - \boldsymbol{a_m}) u_j^{\kappa'}(\boldsymbol{a_m}) - \omega^2 u_i^{\kappa}(\boldsymbol{a_n}) = 0, \tag{1}$$

where superscripts  $\kappa$ ,  $\kappa'$  note two sub-lattices A and B, and subscripts i, i = x, v, z take three values corresponding to the space coordinate, the vector  $\mathbf{a}_{\mathbf{m}}$  and  $\mathbf{a}_{\mathbf{n}}$  numerates the lattice cells. The dynamic matrix  $\varphi_{ii}^{\kappa\kappa'}$  can be taken in the following symmetric form:

$$\varphi_{ii}^{AB}(\mathbf{a_n}) = \varphi_{ii}^{BA}(-\mathbf{a_n}),$$

because the potential energy is a quadratic function of the atomic displacements  $u_i^A(\boldsymbol{a_n})$  and  $u_i^B(\boldsymbol{a_n})$ .

Each atom, for instance  $A_0$ , shown in Fig. 1(a), has three first nearest neighbors in the other sub-lattice, i.e. B with the relative

$$\mathbf{B}_1 = a(1,0), \quad \mathbf{B}_{2,3} = a(-1, \mp \sqrt{3})/2,$$

and 6 s nearest neighbors in the same sub-lattice A with the relative vectors

$$\begin{split} \textbf{\textit{A}}_{2,5} &= \pm a \Big(0,\sqrt{3}\Big), \quad \textbf{\textit{A}}_{3,4} = a \Big(-3,\pm\sqrt{3}\Big) \Big/2, \\ \textbf{\textit{A}}_{1,6} &= a \Big(3,\pm\sqrt{3}\Big) \Big/2, \end{split}$$

where a = 1.42 Å is the carbon-carbon distance.

For the first nearest neighbors (in the B sub-lattice), the dynamical matrix has the form of

$$\varphi_{ij}^{AB}(\mathbf{q}) = \sum_{\kappa=1}^{3} \Phi_{ij}^{AB}(\mathbf{B}_{\kappa}) \exp(i\mathbf{q}\mathbf{B}_{\kappa}), \tag{2}$$

and for the next nearest neighbors (in the A sub-lattice)

$$\varphi_{ij}^{AA}(\mathbf{q}) = \Phi_{ij}^{AA}(\mathbf{A}_0) + \sum_{\kappa=1}^{6} \Phi_{ij}^{AA}(\mathbf{A}_{\kappa}) \exp(i\mathbf{q}\mathbf{A}_{\kappa}), \tag{3}$$

where  $A_0$  is the atom chosen at the center of the coordinate system in the A sub-lattice and the wave vector  $\mathbf{q}$  is taken in units of 1/a.

To obtain the dynamical matrix, we use a transformation with variables  $\xi$ ,  $\eta = x \pm iy$  transforming under the rotation  $C_3$  around the z-axis as follows  $(\xi, \eta) \rightarrow (\xi, \eta) \exp(\pm 2\pi i/3)$ . In intrinsic graphene, the honeycomb lattice has the symmetry of the point group  $D_{6h}$ . But with an in-plane electric field, the symmetry breaks to  $D_{2h}$ which is generated by  $(\sigma_v, \sigma_z)$ . Since the complexity of the analysis of the relative direction of the external field and the vector of the lattice, to simplify the situation we assume the in-plane electric field is along the vector A<sub>0</sub>B<sub>1</sub>. Considering the reflection by the xz Here is along the vector  $A_0B_1$ . Considering the reflection by the xz plane  $\sigma_v$ , note  $\Phi_{\xi\eta}^{AB}(B_1)\equiv\alpha$ ,  $\Phi_{\xi\eta}^{AB}(B_2)\equiv\alpha'$ ,  $\Phi_{\xi\eta}^{AB}(B_1)\equiv\beta$ ,  $\Phi_{\xi\xi}^{AB}(B_2)\equiv\beta'$ ,  $\Phi_{\xi\xi}^{AB}(A_1)\equiv\delta$ ,  $\Phi_{\xi\xi}^{AA}(A_2)\equiv\delta'$ ,  $\Phi_{\xi\eta}^{AA}(A_3)\equiv\delta''$ ,  $\Phi_{\xi\eta}^{AA}(A_1)\equiv\gamma$ ,  $\Phi_{\xi\eta}^{AA}(A_2)\equiv\gamma'$ ,  $\Phi_{\xi\eta}^{AA}(A_3)\equiv\gamma'$ , and we have  $\Phi_{\xi\eta}^{AA}(A_0)=0$ .

The force constant  $\Phi_{\xi\eta}^{AA}(A_0)$  can be eliminated with the help of conditions improved by improved the conditions improved by improved the conditions improved by improved the conditions in the conditions improved the conditions in the condit

conditions imposed by invariance with respect to the translations of the layer as a whole in the x direction. Using the equations of motion (1) and Eqn. (2) and (3), considering the symmetry of space translation we have

$$\Phi_{\varepsilon_n}^{AA}(A_0) + \alpha + 2\alpha' + 2\gamma' + 2\gamma'' = 0.$$

In the first and second nearest neighbor approximation, the corresponding dynamical matrix for the in-plane modes has the form

$$\varphi^{AA}(q) = \begin{pmatrix} \varphi_{\xi\eta}^{AA}(q) & \varphi_{\xi\xi}^{AA}(q) \\ \varphi_{\xi\xi}^{AA}(q)^* & \varphi_{\xi\eta}^{AA}(q)^* \end{pmatrix}, \tag{4}$$

$$\varphi^{AB}(q) = \begin{pmatrix} \varphi_{\xi\eta}^{AB}(q) & \varphi_{\xi\xi}^{AB}(q) \\ \varphi_{\xi\xi}^{AB}(q)^* & \varphi_{\xi\eta}^{AB}(q)^* \end{pmatrix}. \tag{5}$$

At the  $\Gamma$  point, the cell of the dynamical matrix can be simplified

$$\begin{array}{ll} \varphi_{\xi\xi}^{AA}(\Gamma) \\ = & 2 {\it Re} \delta ^{\dot{}} + 2 {\it Re} \delta ^{\dot{'}}, \varphi_{\xi\xi}^{AB}(\Gamma) = \beta + 2 {\it Re} \beta ^{\dot{}}, \quad \varphi_{\xi\eta}^{AB}(\Gamma) \\ = & \alpha + 2 {\it Re} \alpha ^{\dot{}}, \qquad \varphi_{\xi\eta}^{AA}(\Gamma) = -\alpha - 2 {\it Re} \alpha ^{\dot{}}. \end{array}$$

Now we can get the optical phonon frequencies for the in-plane branches at  $\Gamma$  point, which are

$$\omega_{TO} = C\sqrt{-\alpha - 2Re\alpha' + \frac{1}{2}\beta + Re\beta' - Re\delta - Re\delta' - Re\delta''},$$
 (6)

$$\omega_{LO} = C\sqrt{-\alpha - 2Re\alpha' - \frac{1}{2}\beta - Re\beta' + Re\delta' + Re\delta' + Re\delta''}.$$
 (7)

The conversion constant from a force constant in dyn/cpn to a

phonon frequency in cm<sup>-1</sup> is given by C = 1.18928  $\left(\frac{cm^{-1}}{dyn}\right)$  [17]. Assuming that the electric field applied on graphene is ignorable to the Hamiltonian of the intrinsic graphene, we can approximate that the response of the phonon energy is linear to the strength of the field, we can get the split of two branches of phonon is

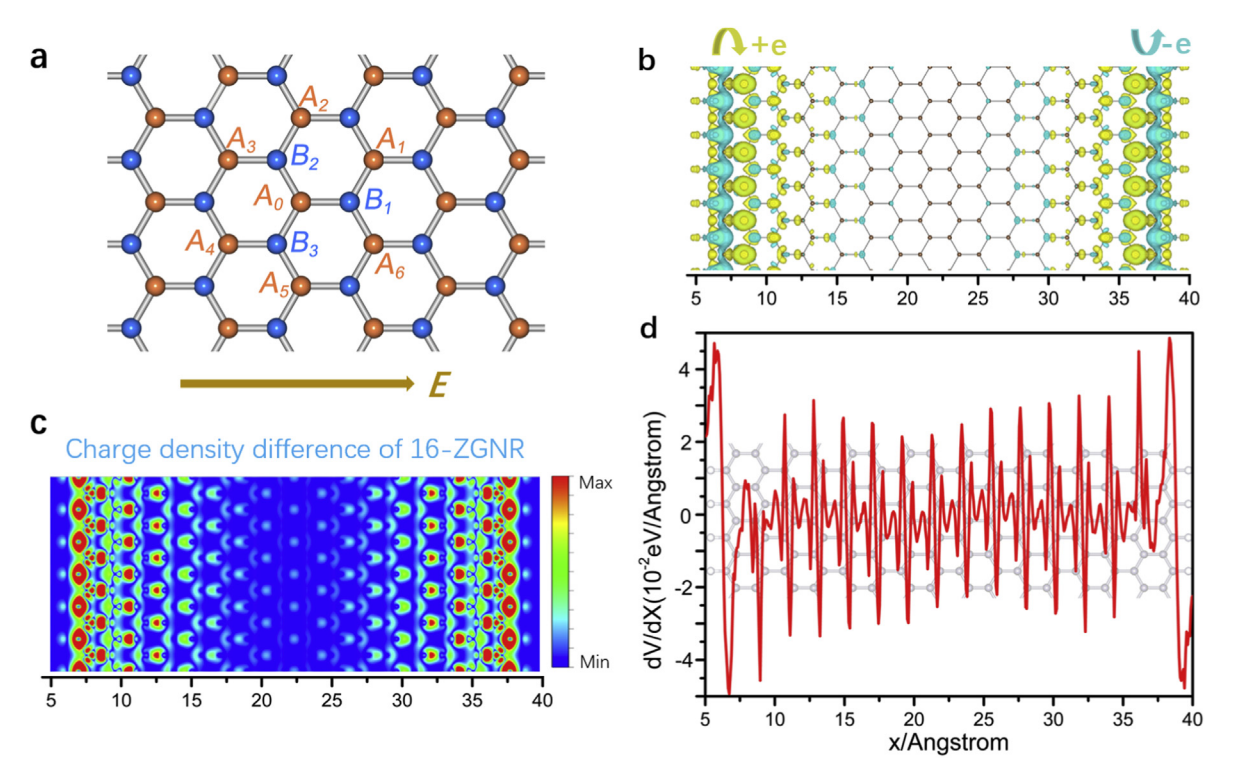


**Fig. 1.** (a) First and second nearest neighbors in the graphene lattice. (b) Polarization charge of graphene under external in-plane electric field. Yellow and cyan iso-charge surfaces respectively represent charge accumulation and depletion at a value of  $0.005e/Å^3$ . (c) Charge density difference of 16-ZGNR. The unit of color bar is  $(e/Å^3)$ . (d) The polarization field of graphene under in-plane electric field, the red curve indicates electric field intensity at different position of 16-ZGNR. (A colour version of this figure can be viewed online.)

$$\Delta\omega = \frac{C\left(\frac{\beta}{2} + Re\beta' - Re\delta - Re\delta' - Re\delta''\right)}{\sqrt{-\alpha - 2Re\alpha'}}$$

$$= \frac{C\left(\frac{\beta}{2} + Re\beta' - Re\delta - Re\delta' - Re\delta''\right)}{\omega_0}, \tag{8}$$

in which the  $\omega_0$  is the energy of optical phonons in intrinsic graphene.

The force constants  $\Phi_{\chi y}^{\alpha\beta}$  are defined as  $\frac{\partial^2 U(r)}{\partial u^\alpha \partial u^\beta}$  [18], where  $u_\chi^\alpha$  denotes the displacement of atom  $\alpha$ . The force constants can be calculated by using density-functional perturbation theory (DFPT) [19,20] where the atomic displacement is taken as a perturbation potential. Eqn. (8) can be rewritten as

$$\Delta\omega = \frac{C}{\omega_0} \left[ \frac{1}{2} \left( \frac{\partial^2 U}{\partial u_x^{A_0} \partial u_x^{B_1}} - \frac{\partial^2 U}{\partial u_y^{A_0} \partial u_y^{B_1}} \right) + \left( \frac{\partial^2 U}{\partial u_x^{A_0} \partial u_x^{B_2}} - \frac{\partial^2 U}{\partial u_y^{A_0} \partial u_y^{B_2}} \right) \right. \\
\left. - \sum_{i=1,2,3} \left( \frac{\partial^2 U}{\partial u_x^{A_0} \partial u_x^{A_i}} - \frac{\partial^2 U}{\partial u_y^{A_0} \partial u_y^{A_i}} \right) \right] \tag{9}$$

The atomic force constants  $\frac{\partial^2 U(r)}{\partial u_p^\alpha \partial u_p^\beta}$  are the second derivatives of the pair potential with respect to the atomic separations, taken at the equilibrium positions. With finite polarization in graphene, atoms in the A sub-lattice and the B sub-lattice have opposite polarization charge. We can note the effective polarization charge of A sub-lattice as  $Q_{eff}$ . With the linear response approximation, the difference of force constants with/without electric field is linear with the effective polarization charge which is linear with the

strength of the field. Expand the force constants with effective charge, Eqn. (9) can be simplified as

$$\Delta\omega \sim \frac{EC}{\omega_0} \left( \frac{1}{2} \frac{\partial Q_{eff}}{\partial u_X^{B_1}} + \frac{\partial Q_{eff}}{\partial u_X^{B_2}} - \sum_{i=1,2,3} \frac{\partial Q_{eff}}{\partial u_X^{A_i}} \right). \tag{10}$$

#### 2.2. Density functional theory (DFT) calculation

The *ab initio* method was used to calculate the polarization charge of graphene under external in-plane electric field, which confirms the breaking of intrinsic chiral symmetry of graphene and the existence of staggered on-site energy on the sub-lattice A and B. Calculations with the VASP package [21–24] were performed in a 16-ZGNR (zigzag graphene nanoribbon) [25–27] to analogize the polarization of infinite graphene [28]. The electric field was imposed perpendicular to the zigzag edge of the nanoribbon supercell [29], shown as Fig. 1(a).

The calculation was performed by using a DFT code, Vienna Abinitio Simulation Package (VASP), within the local-density approximation (LDA). Projector-augmented-wave (PAW) pseudopotentials were used. Plane waves with a kinetic energy cutoff  $E_c$  of 650eV were used as basis sets and 83 irreducible k points ( $N_k = 83$ ) are sampled. Fig. 1(b) shows the calculation result of the polarization of carbon atoms under external in-plane electric field. Yellow and cyan iso-charge surfaces respectively represent charge accumulation and depletion at a value of  $0.005e/\text{Å}^3$ . At the center of the nanoribbon, the polarization is diminished by the screen effect of the polarization charge at the edge. On the other hand, the polarization charge of the atoms at the edges of the nanoribbon accumulate by the configuration restriction. Because of the angle between the orientation of the lattice and the external electric field,

the atom of sub-lattice A appear a different polarization from the atom of sub-lattice B. Since the external field induce a relative polarization between two kinds of atoms, the intrinsic chiral symmetry of graphene is broken. We also calculate the charge density difference of 16-ZGNR, shown as Fig. 1(c), which confirms the existence of staggered on-site energy on the AB sub-lattices. Fig. 1(d) shows electric field intensity at different position of 16-ZGNR. According to fig (c) and (d), it can be clearly seen that the non-zero polarization charge appears at the place where the total electric field is not zero [30,31]. The calculation results show that under non-zero total electric field, there is a relative polarization between the atoms of sub-lattice A and B.

To confirm that these matrix elements break the 6-fold symmetry of single layer graphene due to external in-plane electric field and quantify the split of iTO/iLO phonons, we perform a force constants calculation. As discussed in Eqn. (9), the force constants  $\Phi_{xy}^{\alpha\beta}$  which are defined as  $\frac{\partial^2 U(r)}{\partial u_x^{\alpha}\partial u_y^{\beta}}$ , can be calculated by using density-functional perturbation theory (DFPT) approach with VASP package, which means the split of optical phonons can be calculated according to Eqn. (9). The process of DFT calculation is: First, a full geometry optimization is performed including the optimization of the lattice constants using the VASP package. Once the optimized structure is obtained, force constants of a 5  $\times$  1 supercell of 16-ZGNR can be calculated by using VASP-DFPT approach [32,33]. The DFPT-calculation of force constants at the  $\Gamma$  point in graphene nanoribbons with/without in-plane electric field are performed. The results of DFPT calculations show that the split of iTO and iLO phonons in graphene is about 8 cm<sup>-1</sup> when the applied electric field intensity is  $1 \times 10^6$  V/m (refer to SI for calculation details).

# 3. Experimental results and discussion

#### 3.1. Experimental details

CVD synthesized graphene was transferred to a silicon wafer with a 300 nm thickness thermally grown silica layer. The designed structure is schematically illustrated in Fig. 2(a) with corresponding parameters are marked in Fig. S3(a) (refer to SI). The Raman spectrum of single layer graphene is shown in Fig. S3(b) (refer to SI). Two electrodes and the zigzag circuit pattern (5 nm Ti/80 nm Au)

were fabricated by using the E-beam lithography and following liftoff process, which means that the two electrodes and the zigzag circuit pattern make direct contact with substrate without graphene between them. Square gold electrodes are both  $80 \mu m \times 80 \mu m$  with a gap distance of 100  $\mu m$ . The polarization charge of graphene induced by the external in-plane electric field was conducted away by the zigzag Au electrodes, so that the screen effect [34] could be reduced. The gap between graphene and zigzag circuit pattern in the plane was about 3 nm due to the precision limitation of sample processing technology. A DC electrical source was used to exert external in-plane electric field on the sample. The current was directly applied to the two electrodes and the zigzag circuit pattern, which does not make direct contact with the graphene. Therefore, the electron doping effect can be ignored. A home-built spectrometer was used for obtaining Raman signal, with an iHR550 Raman spectrometer from Horiba working with a 1200 g mm<sup>-1</sup> grating. The objective lens is  $50 \times$  magnifications. Each spectrum is acquired for 20 s, with the purpose of minimizing the noise-to-signal ratio. The laser excitation was 488 nm. The power of the excitation laser was less than 7.5 mW and the spot size of the excitation laser on the sample is about 3  $\mu m$ . When the excitation laser was focused on the measurement points, the spectra were collected until the energy and the intensity of G peak or G<sup>+</sup> and G<sup>-</sup> peaks became stable.

#### 3.2. Results and discussion

Raman spectroscopy is often used to characterize the symmetry of materials, since the vibration frequencies of modes reflect the internal symmetry of the material [35]. G peak in Graphene Raman spectrum corresponds to the two-fold degenerate  $E_{2g}$  mode phonons (iTO and iLO) at the Brillouin-zone center ( $\Gamma$  point) in reciprocal space [36]. When the  $D_{6h}$  symmetry at  $\Gamma$  point is broken, the degeneration of iTO and iLO phonons is eliminated and G peak splits into two peaks, as  $G^+$  peak and  $G^-$  peak. Therefore, the G peak is widely used to directly reflect the change in the symmetry of the graphene, such as the situations of imposing strain [37], temperature [38] and molecular adsorption [39]. Since the split of  $G^+$  and  $G^-$  peaks in the Raman spectrum reflects the symmetry broken of the graphene, we can quantize the change of graphene topological

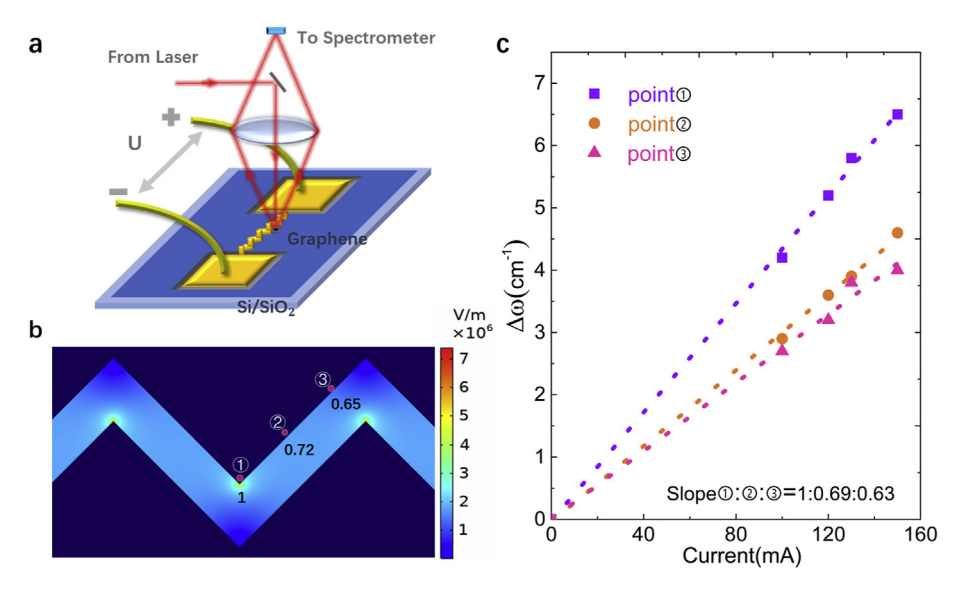


**Fig. 2.** (a) Schematic illustration of the experimental set-up and the graphene sample structure. (b) The simulated in-plane electric field intensity distribution of the tested area. The calculated ratio of the field intensity of the points are also marked. (c)  $\Delta \omega$  as a function of current for points 1, 2 and 3. The straight dotted lines fitting of the three points are also shown with the purple, orange and pink dot lines. (A colour version of this figure can be viewed online.)

property by measuring the split of two peaks.

To measure the effect of polarization charge induced phonon split, an experiment is designed to verify the relationship between external in-plane electric field and the split of iTO and iLO phonons. Schematic illustration of the experimental set-up and the graphene sample structure are shown in Fig. 2(a) with corresponding parameters are marked in Fig. S3(a). Fig. 2(b) shows the different local electric field intensities estimated by the method of COMSOL simulation [40], with three representative points marked specially. In the condition of a macroscale current of 20 mA, the intensity of the local electric field could be as large as about  $5 \times 10^5$  V/m at each corner of the gold structure, while in other places near the gold the intensity is smaller. According to our theoretical results shown as Eqn. (10), we can derive that the split which in the point 1 is the largest, point 2 is smaller while point 3 is the smallest. And the theoretical result is verified by Raman experiment which is shown in Fig. 2(c). The split of  $G^+$  and  $G^-$  peaks  $\Delta \omega$ , which is fitted by the experiment data measured at the point of 1, 2, and 3, is shown by dotted lines with different color for each point as a linear function of current in Fig. 2(c). Among the three points, the Raman spectrum of each special point at certain current intensity was measured several times to get the average. Since the strength of current used in the experiment is just proportional to the intensity of the external in-plane field in microscale,  $\Delta \omega$  is proportional to the intensity of external in-plane electric field. The slopes of three dashed lines reflect the relative degree of split, that is, the one of point 1 is the largest and the one of point 2 is smaller while point 3 is the smallest, which agrees well with theoretical model.

To verify the theory further, we conduct a detailed analysis of the experimental data. Black solid lines in Fig. 3(a) shows the G peak of the point 1 as a function of the electric current which ranging from 0 to 150 mA. The experimental result shows the G peak is red-shifted with the increase of the current intensity. As the

in-plane electric field intensity increases in proportion to current, the G peak is red-shifted with the increase of electric field intensity. Besides, it shows an enlarged split of G<sup>-</sup> peak and G<sup>+</sup> peak with a rate of 1 wavenumber by 22 mA. The details of the other two points are shown in Fig S (4). According to our COMSOL simulation results, the intensity of local electric field could be as large as about  $6 \times 10^6$  V/m when applied current strength is 150 mA. It can be seen from Fig. 3(a) that the split of G peak is about 6.8 wavenumbers when current strength is 150 mA, which means  $\Delta\omega$  is  $6.8 \text{ cm}^{-1}$  when electric field intensity is about  $6 \times 10^6 \text{ V/m}$  in our experiment. As pointed out in DFPT calculation results, the split of iTO and iLO phonons in graphene is about 8 cm<sup>-1</sup> when the applied electric field intensity is  $1 \times 10^6$  V/m, which indicates that the calculation results are consistent with experimental results in microscale. Because of the high quality of our graphene, the signal of D peak is weak and hardly detected. In addition to the G peak, we also performed the development of Raman spectra of the 2D peak with the current intensity. The result shows that there is little impact on the Raman spectra of the 2D peak as the current increasing. The development of Raman spectra of the 2D peak with the current intensity is shown in Fig. S5(refer to SI).

We demonstrate that the split of G peak is reversible by means of electrically controlling. We measured the Raman spectrum of single layer graphene with the applied current strength ranging from 0 to 150 mA. Fig. 3(b) shows Raman shifts of G peak in single layer graphene with current strength ranging from 0 to 150 mA. The measurement results show that the G peak of graphene blue shifts when current increases from 0 to 150 mA, and then red shifts when current decreases to 0. It can be seen clearly that G peak splits into  $G^-$  peak and  $G^+$  peak when current strength is 150 mA, and then the split of G peak disappears when current strength decreases to 0, which implies the split of G peak is reversible by means of applying an external in-plane electric field.

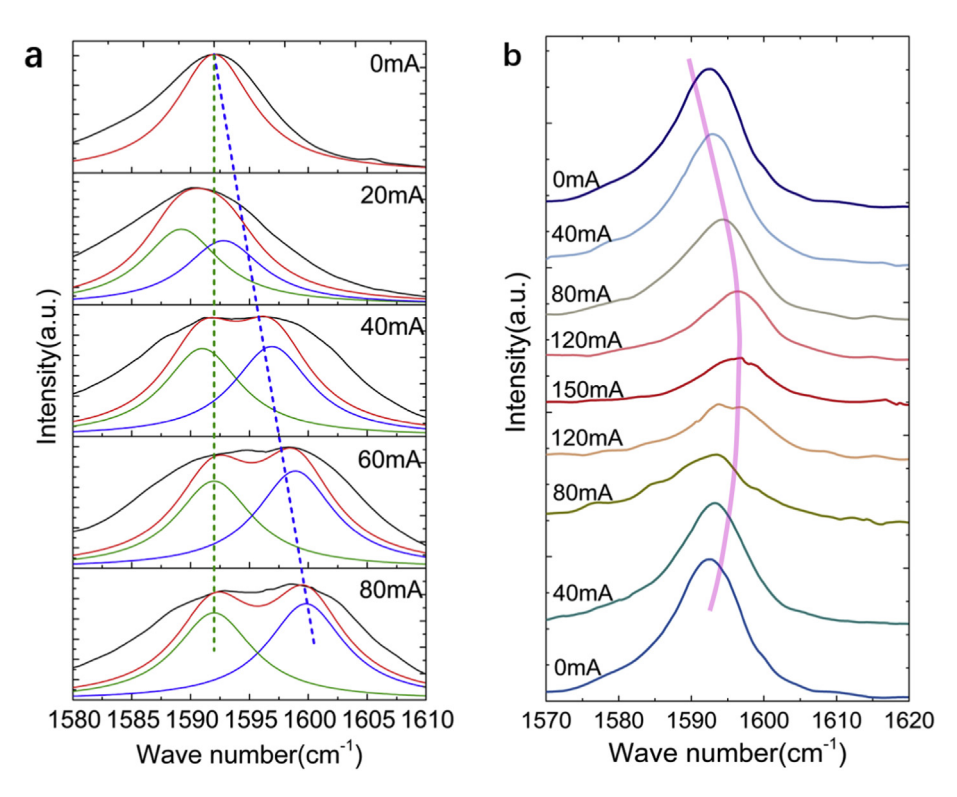


**Fig. 3.** (a) Raman spectra (black) and fitting (red line, overlapped by two Lorentz line shape curves) of the point 1 with the current ranging from 0 to 150 mA. The green curve and the blue represent the fitted  $G^-$  peak and  $G^+$  peak, respectively. (b) Raman shifts of G peak in single layer graphene with current ranging from 0 to 150 mA. (A colour version of this figure can be viewed online.)

Thermal effect can be excluded in this experiment. Many previous researches show that the positions of G peak and 2D peak in single layer graphene red shift as temperature increasing [41–43]. Because the G peak position blue shifts with increasing current and the 2D peak position changes little, we can conclude that the Raman shift in our experiment is unlikely caused by temperature.

We also studied the polarization dependence of the intensity of G<sup>+</sup> and G<sup>-</sup> Raman spectrum to exclude the existence of strain. The split of G peak in single layer graphene can also be caused by strain. The strain-induced G peak splitting exhibits polarization dependence when detecting the Raman spectrum intensity of G<sup>+</sup> and G<sup>-</sup> peak with linear polarized light. The intensity of G<sup>+</sup> and G<sup>-</sup> peak is dependent on the angle between the incident light polarization and the strain axis [37]. In this research, the inversion symmetry breaking of single layer graphene is due to the application of an external in-plane electric field, which induces the G peak splitting. To exclude the existence of strain, we performed the polarization measurements by rotating the angle between the incident polarized light and the initial laser polarization axis. However, The result of our measurements shows that the intensity of G<sup>+</sup> and G<sup>-</sup> peak doesn't change along with the angle (refer to SI Fig. S6), which implies there is almost little polarization dependence. Therefore, the split of G peak in single layer graphene is unlikely caused by strain in this research.

#### 4. Conclusions

In summary, we demonstrate that the relative polarization charge can be utilized to manipulate the internal symmetry of graphene, which the existence of the polarization charge is verified by using the DFT calculation. A quantitative theoretical analysis reveals that the split of G peak induced by inversion symmetry breaking is linearly with the external in-plane electric field intensity, which is verified by Raman experiment. The measured  $\Delta\omega$  can reach 6.8 cm $^{-1}$  when the applied current strength is 150 mA.

We believe that the way of symmetry manipulation by in-plane external electric field method and the corresponding Raman spectroscopy method of characterization advance fundamental comprehension for the inner mechanism of topological phase transition of graphene. Furthermore, this research is referential to application of topological non-trivial materials based on graphene. It provides the possibility of studying artificial valley polarized materials and a method to generate and measure a topological non-trivial state of graphene by manipulate the symmetry of graphene with sub-lattice contrasted polarization, which can be applied in the realm of valley electronic devices and graphene based semi-conductor devices in the future.

#### 4.1. Methods

#### 4.1.1. Graphene growth

Graphene film was synthesized on the surface of electrochemically polished Cu foil (Alfa-Aesar #46965) in a low pressure CVD (LPCVD) system equipped with a 1 in. Diameter quartz tube. Before graphene growth, Cu foil was heated to 1020 °C and then annealed under H2 atmosphere (100 sccm, ~100 Pa) for 1 h to eliminate the surface oxygen and contamination. Then, rapid growth of large single-crystal graphene was fulfilled via second passivation and multistage carbon supply strategy.

#### 4.1.2. Numerical simulations

The simulated in-plane electric field intensity distribution of Zigzag circuit pattern was performed by using the finite element solver (COMSOL). The simulation domain includes the structure with perfect matched layers in the direction of applying a positive

electric field. The dielectric constant of Au and is  $1\times 10^7$  and the air is 1. The physical field interface is the electric currents (ec), and the intensity of the current applied on two electrodes is ranging from 0 to 150 mA.

#### **Declaration of competing interest**

The authors declare that they have no known competing financial interests or personal relationships that could have appeared to influence the work reported in this paper.

#### **CRediT authorship contribution statement**

Beibei Shi: Investigation, Validation, Formal analysis, Writing - original draft, Software, Visualization, Writing - review & editing. Yingdong Xiao: Conceptualization, Methodology, Writing - original draft. Tianyang Han: Investigation, Data curation, Visualization. Haotian Cheng: Software. Jincan Zhang: Resources. Qiao Jiang: Formal analysis. Hailin Peng: Resources. Han Zhang: Writing - review & editing, Funding acquisition. Xing Zhu: Supervision, Writing - review & editing. Zheyu Fang: Writing - review & editing, Supervision, Project administration, Funding acquisition.

#### Acknowledgements

This work is supported by the National Key Research and Development Program of China (grant no. 2019YFA0210203, 2017YFA0205700,2017YFA0206000), National Science Foundation of China (grant nos. 11674012, 61521004, 21790364, 61422501, and 11374023), Beijing Natural Science Foundation (grant nos. Z180011, and L140007), and Foundation for the Author of National Excellent Doctoral Dissertation of China (grant no. 201420), National Program for Support of Top-notch Young Professionals (grant no. W02070003), and High-performance Computing Platform of Peking University.

### Appendix A. Supplementary data

Supplementary data to this article can be found online at https://doi.org/10.1016/j.carbon.2020.03.018.

#### References

- [1] Y. Shimazaki, M. Yamamoto, I.V. Borzenets, K. Watanabe, T. Taniguchi, S. Tarucha, Generation and detection of pure valley current by electrically induced Berry curvature in bilayer graphene, Nat. Phys. 11 (2015) 1032–1036.
- [2] S.F. Wu, Jason S. Ross, Gui-Bin Liu, Grant Aivazian, Aaron Jones, Zaiyao Fei, et al., Electrical tuning of valley magnetic moment through symmetry control in bilayer MoS2, Nat. Phys. 9 (2013) 149–153.
- [3] D. Pesin, A.H. MacDonald, Spintronics and pseudospintronics in graphene and topological insulators, Nat. Mater. 11 (2012) 409–416.
- [4] J. Li, K. Wang, K.J. McFaul, Z. Zern, Y.F. Ren, K. Watanabe, et al., Gate-controlled topological conducting channels in bilayer graphene, Nat. Nanotechnol. 11 (2016) 1060–1065.
- [5] D. Xiao, M.-C. Chang, Q. Niu, Berry phase effects on electronic properties, Rev. Mod. Phys. 82 (2010) 1959.
- [6] Y. Chen, J.G. Analytis, J.-H. Chu, Z.K. Liu, S.-K. Mo, X.L. Qi, et al., Experimental realization of a three-dimensional topological insulator, Bi2Te3, Science 325 (2009) 178–181.
- [7] Jinsong Zhang, Cui-Zu Chang, Peizhe Tang, Zuocheng Zhang, Feng Xiao, Li Kang, et al., Topology-driven magnetic quantum phase transition in topological insulators, Science (2013), 1232003.
- [8] E. D'Elia, H.S. Ahmed, E. Feilden, E. Saiz, Electrically-responsive graphene-based shape-memory composites, Appl. Mater. Tod. 15 (2019) 185–191.
- [9] H. Wang, Z. Xing, Z. Hu, Y. Zhang, Y. Hu, Y. Sun, et al., Sn-based submicronparticles encapsulated in porous reduced graphene oxide network: advanced anodes for high-rate and long life potassium-ion batteries, Appl. Mater. Tod. 15 (2019) 58–66.
- [10] A.K. Geim, K.S. Novoselov, The rise of graphene, Nanosci. Technol. (2009) 11–19.
- [11] D.L. Miller, K.D. Kubista, G.M. Rutter, M. Ruan, Walt A. de Heer, Phillip N. First,

- et al., Observing the quantization of zero mass carriers in graphene, Science 324 (2009) 924–927.
- [12] E.V. Castro, K.S. Novoselov, S.V. Morozov, N.M.R. Peres, J.M.B. Lopes dos Santos, Johan Nilsson, et al., Biased bilayer graphene: semiconductor with a gap tunable by the electric field effect, Phys. Rev. Lett. 99 (2007), 216802.
- [13] J. Slawinska, I. Zasada, Z. Klusek, Energy gap tuning in graphene on hexagonal boron nitride bilayer system, Phys. Rev. B 81 (2010), 155433.
- [14] K.V. Emtsev, F. Speck, Th Seyller, L. Ley, J.D. Riley, Interaction, growth, and ordering of epitaxial graphene on SiC{0001} surfaces: a comparative photoelectron spectroscopy study, Phys. Rev. B 77 (2008), 155303.
- [15] L.A. Falkovsky, Symmetry constraints on phonon dispersion in graphene, Phys. Lett. 372 (2008) 5189.
- [16] L.A. Falkovsky, Phonon dispersion in graphene, J. Exp. Theor. Phys. 105 (2007) 397–403
- [17] A. Grüneis, R. Saito, T. Kimura, L.G. Cançado, M.A. Pimenta, A. Jorio, et al., Determination of two-dimensional phonon dispersion relation of graphite by Raman spectroscopy, Phys. Rev. B 65 (2002), 155405.
- [18] L. Wirtz, A. Rubio, The phonon dispersion of graphite revisited, Solid State Commun. 131 (2004) 141–152.
- [19] Stefano Baroni, Stefano de Gironcoli, Andrea Dal Corso, Paolo Giannozzi, Phonons and related crystal properties from density-functional perturbation theory, Rev. Mod. Phys. 73 (2001) 515.
- [20] Xavier Gonze, First-principles responses of solids to atomic displacements and homogeneous electric fields: implementation of a conjugate-gradient algorithm, Phys. Rev. B 55 (1997) 10337.
- [21] P.E. Blochl, Projector augmented-wave method, Phys. Rev. B 50 (1994) 17953.
- [22] G. Kresse, J. Furthmuller, Efficient iterative schemes for ab initio total-energy calculations using a plane-wave basis set, Phys. Rev. B 54 (1996) 11169.
- [23] G. Kresse, D. Joubert, From ultrasoft pseudopotentials to the projector augmented-wave method, Phys. Rev. B 59 (1999) 1758.
- [24] P.M. Perez-Piskunow, G. Usaj, C.A. Balseiro, L.E.F. Foa Torres, Floquet chiral edge states in graphene, Phys. Rev. B 89 (2014), 121401.
- [25] S. Dutta, S.K. Pati, Novel properties of graphene nanoribbons: a review, I. Mater. Chem. 10 (2010) 1039.
- [26] Li Yang, Cheol-Hwan Park, Young-Woo Son, Marvin L. Cohen, Steven G. Louie, Quasiparticle energies and band gaps in graphene nanoribbons, Phys. Rev. Lett. 99 (2007), 186801.
- [27] Kyoko Nakada, Mitsutaka Fujita, Gene Dresselhaus, S. Mildred, Dresselhaus, Edge state in graphene ribbons: nanometer size effect and edge shape dependence, Phys. Rev. B 54 (1996), 17954.
- [28] A.H. Castro Neto, F. Guinea, N.M.R. Peres, K.S. Novoselov, A.K. Geim, The electronic properties of graphene, Rev. Mod. Phys. 81 (2009) 109.
- [29] Y-Woo Son, M.L. Cohen, S.G. Louie, Half-metallic graphene nanoribbons,

- Nature 444 (2006) 347-349.
- [30] R.S. Akzyanov, A.O. Sboychakov, A.V. Rozhkov, A.L. Rakhmanov, Franco Nori, AA-stacked bilayer graphene in an applied electric field: tunable antiferromagnetism and coexisting exciton order parameter, Phys. Rev. B 90 (2014), 155415.
- [31] Y.P. Wang, X.G. Li, J.N. Fry, Hai-Ping Cheng, First-principles studies of electric field effects on the electronic structure of trilayer graphene, Phys. Rev. B 94 (2016), 165428.
- [32] H. Wang, Y. fang Wang, Vibrational properties of graphene and graphene layers, J. Raman Spectrosc. 40 (2009).
- [33] O. Dubay, G. Kresse, Accurate density functional calculations for the phonon dispersion relations of graphite layer and carbon nanotubes, Phys. Rev. B 67 (2004), 035401.
- [34] Elton J.G. Santos, E. Kaxiras, Electric-field dependence of the effective dielectric constant in graphene, Nano Lett. 13 (2013) 898–902.
- [35] Xin Cong, Qiao-Qiao Li, Xin Zhang, Miao-Ling Lin, Jiang-Bin Wu, Xue-Lu Liu, et al., Probing the acoustic phonon dispersion and sound velocity of graphene by Raman spectroscopy, Carbon 149 (2019) 19–24.
- [36] A.C. Ferrari, J.C. Meyer, V. Scardaci, C. Casiraghi, M. Lazzeri, F. Mauri, et al., Raman spectrum of graphene and graphene layers, Phys. Rev. Lett. 97 (2006), 187401.
- [37] T.M.G. Mohiuddin, A. Lombardo, R.R. Nair, A. Bonetti, G. Savini, R. Jalil, et al., Uniaxial strain in graphene by Raman spectroscopy: G peak splitting, Grüneisen parameters, and sample orientation, Phys. Rev. B 79 (2009), 205433.
- [38] I. Calizo, A.A. Balandin, W. Bao, F. Miao, C.N. Lau, Temperature dependence of the Raman spectra of graphene and graphene multilayers, Nano Lett. 75 (2007) 2645.
- [39] N. Jung, A.C. Crowther, Namdong Kim, Philip Kim, Louis brus, Raman enhancement on graphene: adsorbed and intercalated molecular species, ACS Nano 4 (2010) 7005.
- [40] T.V. Tsoulos, L. Han, J. Weir, H.L. Xin, L. Fabris, A closer look at the physical and optical properties of gold nanostars: an experimental and computational study. Nanoscale 11 (2017) 3766—3773.
- [41] I. Calizo, A.A. Balandin, W. Bao, F. Miao, C.N. Lau, Temperature dependence of the Raman spectra of graphene and graphene multilayers, Nano Lett. 7 (2007) 2645—2649.
- [42] Haiqing Zhou, Caiyu Qiu, Yu Fang, Huaichao Yang, Minjiang Chen, Lijun Hu, et al., Raman scattering of monolayer graphene: the temperature and oxygen doping effects, J. Phys. D Appl. Phys. 44 (2011), 185404.
- 43] L.M. Malard, R.L. Moreira, D.C. Elias, F. Plentz, E.S. Alves, M.A. Pimenta, Thermal enhancement of chemical doping in graphene: a Raman spectroscopy study, J. Phys. Condens. Matter 22 (2010) 334202.